Bacteriophage cooperation suppresses CRISPR-Cas3 and Cas9 immunity

Adair L. Borges[1], Jenny Y. Zhang[1], MaryClare Rollins[2], Beatriz A. Osuna[1], Blake Wiedenheft[2], Joseph Bondy-Denomy[1,3*]

[1]Department of Microbiology and Immunology, University of California San Francisco, CA 94143, USA
[2] Department of Microbiology and Immunology, Montana State University, Bozeman, MT 59717, USA.
[3]Quantitative Biosciences Institute, University of California San Francisco, CA 94143, USA

*Correspondence: joseph.bondy-denomy@ucsf.edu

SUMMARY

Bacteria utilize CRISPR-Cas adaptive immune systems for protection from bacteriophages (phages), and some phages produce anti-CRISPR (Acr) proteins that inhibit immune function. Despite thorough mechanistic and structural information describing the mode-of-action for Acr proteins, how they are deployed by phages during infection is unknown. Here, we show that Acr production does not guarantee phage replication, but instead, CRISPR-Cas neutralization and phage infections fail when phage population numbers are too low. Failing infections can be rescued by kin phages acting as Acr producers, demonstrating that infections succeed if a sufficient Acr dose is contributed to a single cell by multiple phage genomes. The production of Acr proteins by phage genomes that fail to replicate leave the cell immunosuppressed, assisting other phages in the population. These observations apply generally to both Cas3 and Cas9-based adaptive immunity. This "cooperative phage" mechanism for CRISPR-Cas inhibition demonstrates inter-virus cooperation that may find parallels in other host-parasite interactions.

INTRODUCTION

Bacteria and the viruses that infect them (phages) are engaged in an ancient evolutionary arms race, which has resulted in the emergence of a diversity of CRISPR-Cas (clustered regularly interspaced short palindromic repeats and CRISPR-associated genes) adaptive immune systems (Koonin et al., 2017). CRISPR-Cas immunity is powered by the acquisition of small fragments of phage genomes into the bacterial CRISPR array, the subsequent transcription and processing of these arrays to generate small CRISPR RNAs, and the RNA-guided destruction of the phage genome (Barrangou et al., 2007; Brouns et al., 2008; Garneau et al., 2010; Levy et al., 2015). The destruction of foreign DNA by CRISPR-Cas has been shown to prevent the acquisition of plasmids, DNA from the environment, phage lytic replication, and prophage integration (Barrangou et al., 2007; Bikard et al., 2012; Cady et al., 2012; Edgar and Qimron, 2010; Garneau et al., 2010). In bacterial populations, these systems provide a fitness advantage to their host microbe during times of phage presence in the environment (van Houte et al., 2016; Westra et al., 2015).

To combat the potent action of RNA-guided CRISPR-Cas nucleases, phages have developed inhibitor proteins called anti-CRISPRs (Acrs). Acr proteins have been discovered that inhibit Type I-F (Bondy-Denomy et al., 2013; Pawluk et al., 2016b) and Type I-E (Pawluk et al., 2014) CRISPR-Cas3 systems, and also the Type II-A (Hynes et al., 2017; Rauch et al., 2017) and Type II-C (Pawluk et al., 2016a) CRISPR-Cas9 systems, across many distinct organisms (Borges et al., 2017; Pawluk et al., 2017). These proteins are likely ubiquitous in coevolving populations of bacteria and phages (Pawluk et al., 2017) and provide a significant replicative advantage to phages in the presence of CRISPR immunity (van Houte et al., 2016).

Anti-CRISPRs were first identified in phages that neutralize the *Pseudomonas aeruginosa* type I-F system (anti-CRISPR type I-F, AcrIF1-5)(Bondy-Denomy et al., 2013), and five more I-F anti-CRISPRs (AcrIF6-10) were subsequently identified in various mobile genetic elements (Pawluk et al., 2016b). The I-F Csy surveillance complex (also called Cascade) is comprised of four proteins (Csy1-4) and a *trans*-acting nuclease/helicase protein, Cas3 (Rollins et al., 2017; Wiedenheft et al., 2011). Anti-CRISPR proteins function by interacting directly with the Csy complex or Cas3, inhibiting DNA binding or cleavage by the immune system (Bondy-Denomy et al., 2015a). The structures of type I-F Acr proteins AcrIF1, AcrIF2, and AcrIF3 have been solved in complex with their target proteins, revealing mechanistically distinct inhibitors that bind tightly to their target Cas protein (Chowdhury et al., 2017; Guo et al., 2017; Maxwell et al., 2016; Wang et al., 2016). Together with the recent identification and characterization of proteins that inhibit Cas9, a common theme in Acr function has been revealed; all characterized Acr proteins are direct stoichiometric interactors of Cas proteins, blocking either phage DNA binding or cleavage (Dong et al., 2017; Harrington et al., 2017; Pawluk et al., 2016a; Rauch et al., 2017).

Despite a detailed mechanistic understanding, however, it is unknown how anti-CRISPR proteins are deployed by phages *in vivo*. During phage infection, we hypothesized that successful inhibition of CRISPR-Cas immunity by Acr proteins would be challenging, as all components of the *P. aeruginosa* immune system are expressed prior to phage infection (Bondy-Denomy et al., 2013; Cady et al., 2012). Where phage DNA cleavage has been assessed *in vivo*, it occurs in as little as 2 minutes (Garneau et al., 2010),

80 suggesting that CRISPR attack may outpace the ability of *de novo* Acr synthesis and
81 action.
82
83 Here, we utilize the diverse array of AcrIF proteins encoded by phages to demonstrate
84 that CRISPR-Cas inactivation is, in fact, a challenge, and that the sufficient
85 concentration of Acr proteins necessary to inactivate CRISPR-Cas is contributed by
86 multiple phage genomes. While initial phage infections may fail, due to the rapid action
87 of the CRISPR-Cas system, immunosuppression can result due to the production of Acr
88 proteins, which benefits phage in the community, leading to a population-level benefit for
89 other phages. We propose that pathogens can contribute to the "remodeling" of their
90 host cell via rapid protein production, even if the initial infecting genomes are cleared,
91 opening the door for their clones.
92
93 **RESULTS**
94 **Anti-CRISPR proteins are imperfect CRISPR-Cas inhibitors**
95 We sought to utilize the diversity of *acr* genes encoded by phages infecting *P.*
96 *aeruginosa* to determine the mechanism of CRISPR-Cas neutralization during infection.
97 Five natural phages, each encoding a single *acrIF* gene, were selected to represent
98 *acrIF1-IF4* and *acrIF7* (*acrIF5* does not exist as the sole *acrIF* gene on any phage,
99 *acrIF6, F8-F10* are not encoded by this phage family). Three of these five phages
100 exhibited reduced efficiency of plaquing (EOP) on *P. aeruginosa* strain wild-type (WT)
101 PA14, possessing a type I-F CRISPR-Cas system, relative to a ΔCRISPR strain (Figure
102 1A, WT:pEmpty). Overexpression of a targeting crRNA (WT:pSp1) exacerbated anti-
103 CRISPR inefficiency, limiting the replication of all anti-CRISPR phages by at least one
104 order of magnitude. This suggests that anti-CRISPR proteins are unable to fully protect
105 their associated phage genome.
106
107 To assess anti-CRISPR strength directly, an isogenic phage panel was generated by
108 replacing the *acrIE3* gene of phage DMS3m with single *acrIF* genes *F1-F7* ($DMS3m_{acrIF1}$-
109 $DMS3m_{acrIF7}$, Figure S1). WT PA14 (1 spacer targeting DMS3m, "1sp") and a laboratory
110 evolved strain (5 spacers targeting DMS3m, "5sp") were challenged with the
111 recombinant phages, revealing that all anti-CRISPRs are quantitatively imperfect during
112 infection (Figure 1B). For phages encoding *acrIF1, F2, F3, F6* or *F7*, >90% of phage in
113 the population failed to replicate (EOP=10^{-1}) when faced with 5 targeting spacers. *acrIF4*

114 and *F5* were very weak, with 99.0-99.99% of phages failing to replicate (EOP=10^{-2}-10^{-4}),
115 depending on the CRISPR spacer content. We conclude that phages encoding *acrs*
116 remain sensitive to CRISPR-Cas immunity, suggesting that anti-CRISPR deployment
117 and action is an imperfect process.
118
119 Given the observation above of two groups of "strong" and "weak" Acr proteins, we
120 selected a two representative AcrIF proteins for downstream experiments, with AcrIE3
121 as a negative control. AcrIF1 was selected as a model strong inhibitor, as its mechanism
122 and binding affinity are known (Csy complex binding, $K_D = 2.5 \times 10^{-11}$ M)(Bondy-Denomy
123 et al., 2015b; Chowdhury et al., 2017). In contrast, AcrIF4 is a weak inhibitor that also
124 binds the Csy complex (Bondy-Denomy et al., 2015a), but with a significantly slower on-
125 rate and faster off-rate compared to AcrIF1 (Figure 1C, Figure S2).
126
127 We next sought to assess the survival of bacterial cell populations over time, when
128 infected with phages that must deploy Acr proteins, but where apparently only a minority
129 of the population actually replicates. Phages were locked in the lytic cycle for the
130 purpose of this experiment, by knocking out the *C repressor* gene (*gp1*) in DMS3m$_{acrIF1}$,
131 DMS3m$_{acrIF4}$, and DMS3m$_{acrIE3}$. The virulent (vir) phages were used at varying
132 concentrations to infect 5sp strains in liquid culture. In the presence of CRISPR
133 immunity, phage replication and bacterial death only occurred at multiplicities of infection
134 (MOI, input plaque forming units per colony forming unit) greater than 0.02 for the strong
135 *acrIF1* (Figure 2A) and greater than an MOI of 2.0 ($\geq 10^7$ PFU) for the weak *acrIF4*
136 (Figure 2B). Despite this high MOI-dependence, no selection or evolution of phage
137 DMS3m$_{acrIF4}$ occurred throughout the experiment, as output phages remained as
138 sensitive to CRISPR-Cas immunity as the input population (Figure S3). The phage
139 encoding *acrIE3* was unable to replicate when faced with CRISPR immunity (Figure 2C),
140 while in the absence of CRISPR, all phages replicated and cleared bacterial cultures
141 similarly (Figure 2D-2F). These data demonstrate that while only a subset of the phage
142 population may replicate, a critical phage concentration threshold exists for any
143 replication to occur. The level of this threshold is inversely proportional to Acr strength,
144 and this determines whether CRISPR-Cas immunity becomes inactivated at the
145 population level.
146
147 **Phage lytic replication requires Acr protein concentration thresholds be met**

148 Concentration-dependent success of CRISPR-Cas neutralization during phage infection
149 could be caused by an excess of phage DNA targets that overwhelm a cell by titrating
150 Csy complexes away from other phages, or by the contribution of Acr proteins from
151 multiple phage genomes in a single cell. To experimentally address these models, we
152 genetically modified phages to render them non-replicative, thus allowing the
153 independent titration of a subset of phages in the population. The immunity region from
154 heteroimmune phage JBD30 (Figure S4A) was introduced into DMS3m phages,
155 generating a hybrid phage, whose replication could be prevented by the overexpression
156 of the JBD30 C repressor (*gp1*, Figure S4B). In the presence of the JBD30 C repressor,
157 high doses of the hybrid phage did not replicate, confirming the efficacy of *gp1*
158 overexpression (Figure S4C). This enabled the mixing of replicative and non-replicative
159 phages, the latter acting as sacrificial genome and Acr donor, to assess the mechanism
160 for the observed concentration dependency.
161
162 In the presence of non-replicating phages encoding *acrIF1*, and possessing the same
163 five DNA target sequences, we observed a striking rescue effect, where this phage
164 assisted in CRISPR-Cas neutralization, enabling $DMS3m_{acrIF1}$ (Figure 2G) and
165 $DMS3m_{acrIF4}$ (Figure 2H) to replicate at input concentrations that are unsuccessful in the
166 absence of the "helper phage". Although the input of helper phages was at a modest
167 level (10^6 PFU, MOI = 0.2), this enabled the replicative phage to achieve an increase of
168 phage titers by 4-5 orders of magnitude. However, this helping effect was not observed
169 when the replicative phage did not encode an AcrIF protein (Figure 2I), or when the non-
170 replicating phage produced *acrIE3* (Figure 2H-2I). Additionally, any potential lysogens
171 formed by the DMS3m hybrid helper phage in this experiment would not have amplified
172 the replicating phage, as these lysogens remain resistant to superinfection (Figure S4D).
173 These data demonstrate that Csy complex titration by infecting phage genomes alone
174 does not appear to be a significant "anti-CRISPR" factor in the outcome of phage
175 replication or bacterial survival. Instead, the determinant of phage replicative success is
176 the concentration of Acr proteins reached in single cells, which is achievable by Acr
177 production from independent phage genomes. This suggests that multiple phage
178 genomes can contribute to the "immunosuppression" of a single host by contributing
179 separate doses of Acr protein, potentially explaining the observed concentration
180 thresholds and inefficiencies observed in plaquing measurements.
181

182 **Lysogeny requires Acr proteins contributed by transient intracellular genomes**
183 All phages encoding Acr proteins that infect *P. aeruginosa* are naturally temperate, and
184 can form lysogens by integrating into the bacterial genome. We therefore measured the
185 impact of CRISPR and Acr proteins on lysogeny establishment during a single round of
186 infection. While previous experiments examined cumulative phage replication in the lytic
187 cycle over many hours, assaying lysogen formation over a short time frame is ideal for
188 understanding the initial events that determine phage genome survival or cleavage.
189 Additionally, lysogeny provides a direct readout for phage genome survival (i.e. an
190 integrated prophage), while in lytic replication, phage survival leads to a dead cell that
191 cannot be recovered. For these experiments, we selected the weak AcrIF4 protein as it
192 provided the largest dynamic range of inefficiency in a single round of infection.
193
194 We generated derivatives of DMS3m$_{acrIF4}$ and DMS3m$_{acrIE3}$ marked with a gentamicin
195 resistance cassette at the end of the genome, replacing a nonessential gene, *gp52*. This
196 allowed the independent titration of two distinct and replicative phage populations and
197 the selection and analysis of stable lysogens after the experiment. These phages were
198 used to infect ΔCRISPR cells (0sp) for a time span less than a single round of infection
199 (50 minutes, Figure S5), and the number of gentamicin resistant lysogens assessed. In
200 the absence of CRISPR selection, a linear increase in the number of lysogens with
201 increasing MOI was observed, over ~4 orders of magnitude (Figure 3A-3B, circles). In
202 the presence of spacers targeting DMS3m (5sp), CRISPR reduced the efficiency of
203 lysogeny (EOL, compared to 0sp) for the weak *acr* phage DMS3m$_{acrIF4}$, to such a degree
204 that lysogeny was undetectable at low MOIs, and impaired by 100-1000-fold at higher
205 MOIs (Figure 3A, triangles). DMS3m$_{acrIF4}$ demonstrated concentration dependence for
206 successful lysogeny, with EOL values below or at the limit of detection for lower MOIs,
207 increasing to EOL = 0.01 at higher MOIs (Figure 3C). Phage DMS3m$_{acrIE3}$ formed no
208 lysogens at all input concentrations tested (Figure 3B, 3D), demonstrating the utility of an
209 *acrIF* gene for lysogen establishment.
210
211 We hypothesized that if the concentration dependence for CRISPR neutralization during
212 lysogeny could also be explained by phage cooperation, the "below-the-threshold"
213 concentration of 10^3 LFU DMS3m$_{acrIF4}$ could be rescued by the addition of helper phages
214 *in trans*. In accordance with this prediction, infection of the 5sp strain with a mixture of
215 DMS3m$_{acrIF4}$ *gp52::gent* phages (10^3 LFU) and 10^7 PFU of unmarked helper phages

216 increased DMS3m$_{acrIF4}$ *gp52::gent* EOL dramatically. EOL increased by 2 orders of
217 magnitude with helper phage DMS3m$_{acrIF1}$ and the DMS3m$_{acrIF4}$ helper phage increased
218 EOL by 1 order of magnitude (Figure 3E). No such increase in lysogeny was observed
219 for a phage without an *acrIF* gene, DMS3m$_{acrIE3}$ *gp52::gent* (Figure 3F). The addition of
220 helper phages DMS3m$_{acrIE3}$, or an escaper phage DMS3m$_{acrIE3}$* had no effect on the
221 EOL of the marked DMS3m$_{acrIF4}$ phage, demonstrating that the helper phage must be an
222 Acr-producer.
223
224 To determine the outcome of this co-infection experiment we used the resulting lysogens
225 as a genetic record of infection success for both the marked phage and the unmarked
226 phage. Importantly, this family of Mu-like phage is capable of integrating randomly in the
227 genome, enabling the formation of polylysogens(Bondy-Denomy et al., 2016). Thus, this
228 allows us to distinguish whether the helper phage genome is still present as a prophage,
229 in addition to the marked prophage which is selected for. All resulting lysogens tested
230 (n=48) possessed only the marked prophage, with none possessing the helper prophage
231 (Figure S6). This demonstrates that the transient presence of the helper phage genome
232 (i.e. no lysogeny) in the same cell was sufficient to generate enough Acr protein to
233 protect the marked phage, leading to the establishment of lysogens that would not exist
234 if not for the helper (Figure 3E, compare “buffer” to “IF1”). The only time rare double
235 lysogens were isolated, was when infecting with marked phage DMS3m$_{acrIE3}$ *gp52::gent*,
236 and an unmarked DMS3m$_{acrIF1}$ helper phage (Figure 3F), since the prophage encoding
237 *acrIE3* would be unable to neutralize CRISPR-Cas after lysogenic establishment and
238 long-lasting protection from the helper prophage was required. Collectively, these data
239 are consistent with a model where the production of Acr proteins from a transient phage
240 genome prior to its cleavage generates an immunosuppressed cell that can be
241 successfully parasitized by another phage upon re- or co-infection(s).
242
243 **Stoichiometric inhibitors of Cas9 required bacteriophage cooperation**
244 The intrinsic inefficiency of stoichiometric inhibitors likely manifests due to the rapid
245 cleavage of a phage genome by CRISPR-Cas complexes, and the need to synthesize
246 the Acr proteins *de novo* during infection. To determine whether this model generally
247 applies to other stoichiometric inhibitors of bacterial immunity, we engineered a *P.*
248 *aeruginosa* strain to express the Cas9 protein from *Streptococcus pyogenes* (SpyCas9)
249 and engineered a DMS3m phage to express a previously identified stoichiometric

250 inhibitor of SpyCas9, AcrIIA4 (Dong et al., 2017; Rauch et al., 2017). In this entirely
251 heterologous experiment, we observed the same inefficiency for a phage relying on an
252 Acr protein. Spot-titration of phage lysates on a strain expressing a single guide RNA
253 (sgRNA) targeting DMS3m decreased the titer of DMS3m$_{acrIE3}$ by many orders of
254 magnitude, while DMS3m$_{acrIIA4}$ was protected (Figure 4A). However, quantification of the
255 efficiency of plaquing again revealed that relying on an Acr protein for replication is
256 imperfect, with an EOP = 0.4 (Figure 4B). In lytic replication infection experiments,
257 DMS3m$_{acrIIA4}$ displayed concentration-dependent replication in the presence of CRISPR
258 targeting (Figure 4C), while DMS3m$_{acrIE3}$ did not replicate in a concentration-dependent
259 manner (Figure 4D). In the absence of CRISPR-Cas targeting, however, both phages
260 replicated robustly (Figure 4E, 4F). To determine whether this concentration dependence
261 to Cas9 inhibition was also a result if insufficient intracellular Acr dose, a non-replicative
262 hybrid DMS3m$_{AcrIIA4}$ phage was generated and used as a helper during infection. Indeed,
263 increased delivery of AcrIIA4 to cells allowed DMS3m$_{AcrIIA4}$ to replicated robustly from a
264 concentration that was previously unsuccessful (Figure 4G), demonstrating phage
265 cooperation to neutralize CRISPR-Cas9. Utilizing a single spacer sequence in this
266 experiment, allowed for phage escape mutations to be more prevalent, and we observed
267 that DMS3m$_{acrIE3}$ could also be helped by increased doses of AcrIIA4 from the phage
268 population (Figure 4H), likely providing enough protection of that phage genome *in trans*
269 to replicate and increase the frequency of escaper phages. This was not seen in
270 previous experiments with 5 spacers targeting the phage, and may represent one
271 example where Acr donations can be "cheated" upon by phages not contributing Acr
272 proteins.
273
274 **DISCUSSION**
275 Here we demonstrate that the necessary intracellular concentration of an anti-immunity
276 protein to achieve inactivation of cellular immunity depends on the relative strengths of
277 both the inhibitor and the immunity pathway, which dictates the number of infecting
278 viruses required in the population. We conclude that a single cell can become
279 immunosuppressed by anti-immune protein contributions from independent infection
280 events. In the absence of viral replication, these infection events serve to contribute to
281 the inactivation of cellular immunity, thus enhancing the probability of successful
282 infection events in the future (Figure 5). We expect that cooperation of this sort is

283 necessary when the immune process acts rapidly and irreversibly on the infecting viral
284 genome, as CRISPR-Cas immunity does.
285
286 The ability of phages to replicate in the lytic cycle or establish lysogens is impacted
287 dramatically by the number of phages in the population. To demonstrate phage-phage
288 cooperation for the deployment of Acr proteins, three distinct genetic strategies were
289 used, allowing the independent titration of phages encoding a defined Acr protein: i) non-
290 replicative Acr donor phages, ii) marked and unmarked phages to follow the fate of only
291 one phage, and iii) the prophage status of lysogens, as a genetic record of phage
292 success. As an experimental tool, restricting the replication of a subset of phages to
293 render them solely as Acr donors allowed the tracking of lytic replication of a "below-the-
294 threshold" concentration of replicative phages. In contrast, the prophage acquisition
295 experiment allows a more natural scenario, where all phages are replicative but an
296 antibiotic resistance marker allows one to track the outcome of one phage genotype,
297 starting at a concentration below its threshold for successful lysogeny. This
298 demonstrated that wild-type helper phages in the population contribute to cellular
299 immunosuppression, enabling the formation of lysogens that did not occur in their
300 absence. The presence of only a single, marked prophage in the bacterial genome
301 proves that the helper phage neither replicated (this would kill the cell), nor lysogenized
302 (prophage would be present), but had been present in the cell transiently.
303
304 The key result here is the observation that phages can remodel their host cell, even in
305 the absence of a replicating or integrated genome. It has long been known that
306 integrated prophages modulate host phenotypes via gene expression, including
307 superinfection exclusion, toxin production, and the production of Acr proteins (Bondy-
308 Denomy et al., 2013; Bondy-Denomy and Davidson, 2014; Bondy-Denomy et al., 2016;
309 Waldor and Mekalanos, 1996; Weigle and Delbruck, 1951). Although less commonly
310 described, there is also precedent for lytic phages to impact an interaction with other
311 phages during replication. The Imm protein produced by the phage T4 prevents other
312 phages in the environment from infecting the cell that one phage is currently replicating
313 within (Lu and Henning, 1989). This has been attributed to preventing superinfection and
314 the potential disruption of the carefully timed phage replication cycle. This supports a
315 conclusion that co- and/or re-infections are a common occurrence in nature. However,
316 here, we propose new model of phage-induced host remodeling; that transient, cleared

genomes produce proteins that could enable future infections, by inactivating defense. This phenomenon would be evolutionarily advantageous in a clonal phage population, where all are providing Acr proteins to neutralize CRISPR, and as shown in Figure 2I, a phage not making an AcrIF protein was unable to “cheat” despite the presence of helper phages in the population.

A distinct, but notable observation from this work is that not all Acr proteins operate at full strength, as AcrIF4 and AcrIF5 provide weak protection to their phage genome. However, encoding these genes still provides a significant advantage to the phage, compared to lacking them entirely. Because the mechanism of action for AcrIF5 is still unknown, we focused on AcrIF4, demonstrating that its affinity for the Csy complex is orders of magnitude lower than stronger Acr proteins like AcrIF1. At present, however, we lack an explanation for why a weak Acr protein would be utilized by phages if stronger variants are available. AcrIF1 was selected as a model strong Acr protein because of its comparable mechanism of action to AcrIF4 (i.e. Csy complex binding). We consider AcrIF1 to be representative for other strong Acr proteins (AcrIF2, F3, F6, F7) as phages encoding them had similar efficiencies of plaquing, and we therefore expect similar threshold concentrations. Going forward, we speculate that the strongest Acr proteins would be enzymatic in nature, allowing rapid and efficient inactivation of CRISPR complexes in a sub-stoichiometric manner, although no such Acr mechanism has been discovered. While not an enzyme, the recent demonstration of the AcrIIC3 protein inactivating two Cas9 proteins at the same time would likely be a more efficient path towards CRISPR neutralization (Harrington et al., 2017).

The challenge of neutralizing a pre-expressed CRISPR-Cas system likely explains why stoichiometric inhibitors like Acr proteins are imperfect, and phages relying on them are partially targeted by CRISPR. The sacrificial, population-level aspect of CRISPR inhibition is reminiscent of the manifestations of CRISPR adaptation in populations of bacterial cells. The majority of infected naïve host cells die, before a clone with a new spacer emerges (Barrangou et al., 2007; Hynes et al., 2014). In the case of anti-immunity, many phages die in order to inhibit CRISPR on a single cell level, and this must happen at sufficient frequency within an ecosystem for phage to prevail. We suspect that this mechanism of cellular immunosuppression and inter-parasite cooperation may have parallels in other host-pathogen interactions, where concentration

351 dependence manifests at predictable levels due the strengths of immune and anti-
352 immune processes.
353
354 **SUPPLEMENTAL INFORMATION**
355 Figures S1-S6 are provided separately.
356
357 **AUTHOR CONTRIBUTIONS**
358 A.L.B. and J.B.D. designed experiments and wrote the manuscript. A.L.B. engineered
359 phage variants and conducted all experiments with the exception of binding affinity
360 measurements. J.Y.Z. assisted with experimental design and execution, phage
361 engineering, and data collection. B.A.O. built the Cas9 strain in *Pseudomonas*
362 *aeruginosa.* J.B.D. supervised experiments. M.R. conducted Acr binding affinity
363 measurements under the supervision of B.W. All authors contributed to data analysis
364 and edited the manuscript.
365
366 **ACKNOWLEDGEMENTS**
367 The Bondy-Denomy lab was supported by the University of California San Francisco
368 Program for Breakthrough in Biomedical Research, funded in part by the Sandler
369 Foundation, and an NIH Office of the Director Early Independence Award (DP5-
370 OD021344). Research in the Wiedenheft lab is supported by the National Institutes of
371 Health (P20GM103500, P30GM110732, R01GM110270, R01GM108888 and R21
372 AI130670), the National Science Foundation EPSCoR (EPS-110134), the M. J. Murdock
373 Charitable Trust, a young investigator award from Amgen, and the Montana State
374 University Agricultural Experimental Station (USDA NIFA).
375

REFERENCES

Barrangou, R., Fremaux, C., Deveau, H., Richards, M., Boyaval, P., Moineau, S., Romero, D.A., and Horvath, P. (2007). CRISPR provides acquired resistance against viruses in prokaryotes. Science *315*, 1709–1712.

Bikard, D., Hatoum-Aslan, A., Mucida, D., and Marraffini, L.A. (2012). CRISPR interference can prevent natural transformation and virulence acquisition during in vivo bacterial infection. Cell Host Microbe *12*, 177–186.

Bondy-Denomy, J., Pawluk, A., Maxwell, K.L., and Davidson, A.R. (2013). Bacteriophage genes that inactivate the CRISPR/Cas bacterial immune system. Nature *493*, 429–432.

Bondy-Denomy, J., and Davidson, A.R. (2014). When a virus is not a parasite: the beneficial effects of prophages on bacterial fitness. J Microbiol *52*, 235–242.

Bondy-Denomy, J., Garcia, B., Strum, S., Du, M., Rollins, M.F., Hidalgo-Reyes, Y., Wiedenheft, B., Maxwell, K.L., and Davidson, A.R. (2015a). Multiple mechanisms for CRISPR-Cas inhibition by anti-CRISPR proteins. Nature *526*, 136–139.

Bondy-Denomy, J., Garcia, B., Strum, S., Du, M., Rollins, M.F., Hidalgo-Reyes, Y., Wiedenheft, B., Maxwell, K.L., and Davidson, A.R. (2015b). Multiple mechanisms for CRISPR-Cas inhibition by anti-CRISPR proteins. Nature *526*, 136–139.

Bondy-Denomy, J., Qian, J., Westra, E.R., Buckling, A., Guttman, D.S., Davidson, A.R., and Maxwell, K.L. (2016). Prophages mediate defense against phage infection through diverse mechanisms. The ISME Journal *10*, 2854–2866.

Borges, A.L., Davidson, A.R., and Bondy-Denomy, J. (2017). The Discovery, Mechanisms, and Evolutionary Impact of Anti-CRISPRs. Annual Review of Virology *4*, annurev–virology–101416–041616.

Brouns, S.J.J., Jore, M.M., Lundgren, M., Westra, E.R., Slijkhuis, R.J.H., Snijders, A.P.L., Dickman, M.J., Makarova, K.S., Koonin, E.V., and van der Oost, J. (2008). Small CRISPR RNAs guide antiviral defense in prokaryotes. Science *321*, 960–964.

Cady, K.C., Bondy-Denomy, J., Heussler, G.E., Davidson, A.R., and O'Toole, G.A. (2012). The CRISPR/Cas adaptive immune system of Pseudomonas aeruginosa mediates resistance to naturally occurring and engineered phages. *194*, 5728–5738.

Chowdhury, S., Carter, J., Rollins, M.F., Golden, S.M., Jackson, R.N., Hoffmann, C., Nosaka, L., Bondy-Denomy, J., Maxwell, K.L., Davidson, A.R., et al. (2017). Structure Reveals Mechanisms of Viral Suppressors that Intercept a CRISPR RNA-Guided Surveillance Complex. Cell *169*, 47–57.e11.

Dong, D., Guo, M., Wang, S., Zhu, Y., Wang, S., Xiong, Z., Yang, J., Xu, Z., and Huang, Z. (2017). Structural basis of CRISPR-SpyCas9 inhibition by an anti-CRISPR protein. Nature.

Edgar, R., and Qimron, U. (2010). The Escherichia coli CRISPR system protects from λ lysogenization, lysogens, and prophage induction. J. Bacteriol. *192*, 6291–6294.

415 Garneau, J.E., Dupuis, M.-È., Villion, M., Romero, D.A., Barrangou, R., Boyaval, P.,
416 Fremaux, C., Horvath, P., Magadán, A.H., and Moineau, S. (2010). The CRISPR/Cas
417 bacterial immune system cleaves bacteriophage and plasmid DNA. Nature *468*, 67–71.

418 Guo, T.W., Bartesaghi, A., Yang, H., Falconieri, V., Rao, P., Merk, A., Eng, E.T.,
419 Raczkowski, A.M., Fox, T., Earl, L.A., et al. (2017). Cryo-EM Structures Reveal
420 Mechanism and Inhibition of DNA Targeting by a CRISPR-Cas Surveillance Complex.
421 Cell *171*, 414–426.e12.

422 Harrington, L.B., Doxzen, K.W., Ma, E., Liu, J.-J., Knott, G.J., Edraki, A., Garcia, B.,
423 Amrani, N., Chen, J.S., Cofsky, J.C., et al. (2017). A Broad-Spectrum Inhibitor of
424 CRISPR-Cas9. Cell.

425 Hynes, A.P., Rousseau, G.M., Lemay, M.-L., Horvath, P., Romero, D.A., Fremaux, C.,
426 and Moineau, S. (2017). An anti-CRISPR from a virulent streptococcal phage inhibits
427 Streptococcus pyogenes Cas9. Nature Microbiology *315*, 1.

428 Hynes, A.P., Villion, M., and Moineau, S. (2014). Adaptation in bacterial CRISPR-Cas
429 immunity can be driven by defective phages. Nature Communications *5*, 4399.

430 Koonin, E.V., Makarova, K.S., and Wolf, Y.I. (2017). Evolutionary Genomics of Defense
431 Systems in Archaea and Bacteria. Annu Rev Microbiol *71*, annurev–micro–090816–
432 093830.

433 Levy, A., Goren, M.G., Yosef, I., Auster, O., Manor, M., Amitai, G., Edgar, R., Qimron,
434 U., and Sorek, R. (2015). CRISPR adaptation biases explain preference for acquisition
435 of foreign DNA. *520*, 505–510.

436 Lu, M.J., and Henning, U. (1989). The immunity (imm) gene of Escherichia coli
437 bacteriophage T4. Journal of Virology *63*, 3472–3478.

438 Maxwell, K.L., Garcia, B., Bondy-Denomy, J., Bona, D., Hidalgo-Reyes, Y., and
439 Davidson, A.R. (2016). The solution structure of an anti-CRISPR protein. Nature
440 Communications *7*, 13134.

441 Pawluk, A., Amrani, N., Zhang, Y., Garcia, B., Hidalgo-Reyes, Y., Lee, J., Edraki, A.,
442 Shah, M., Sontheimer, E.J., Maxwell, K.L., et al. (2016a). Naturally Occurring Off-
443 Switches for CRISPR-Cas9. Cell *167*, 1829–1838.e1829.

444 Pawluk, A., Bondy-Denomy, J., Cheung, V.H.W., Maxwell, K.L., and Davidson, A.R.
445 (2014). A new group of phage anti-CRISPR genes inhibits the type I-E CRISPR-Cas
446 system of Pseudomonas aeruginosa. mBio *5*, e00896–e00896–14.

447 Pawluk, A., Davidson, A.R., and Maxwell, K.L. (2017). Anti-CRISPR: discovery,
448 mechanism and function. Nat Rev Micro *1*, nrmicro.2017.120.

449 Pawluk, A., Staals, R.H.J., Taylor, C., Watson, B.N.J., Saha, S., Fineran, P.C., Maxwell,
450 K.L., and Davidson, A.R. (2016b). Inactivation of CRISPR-Cas systems by anti-CRISPR
451 proteins in diverse bacterial species. Nature Microbiology *1*, 1–6.

452 Rauch, B.J., Silvis, M.R., Hultquist, J.F., Waters, C.S., McGregor, M.J., Krogan, N.J.,

453 and Bondy-Denomy, J. (2017). Inhibition of CRISPR-Cas9 with Bacteriophage Proteins.
454 Cell *168*, 150–158.e10.

455 Rollins, M.F., Chowdhury, S., Carter, J., Golden, S.M., Wilkinson, R.A., Bondy-Denomy,
456 J., Lander, G.C., and Wiedenheft, B. (2017). Cas1 and the Csy complex are opposing
457 regulators of Cas2/3 nuclease activity. Proceedings of the National Academy of
458 Sciences *23*, 201616395–E5121.

459 van Houte, S., Ekroth, A.K.E., Broniewski, J.M., Chabas, H., Ben Ashby, Bondy-
460 Denomy, J., Gandon, S., Boots, M., Paterson, S., Buckling, A., et al. (2016). The
461 diversity-generating benefits of a prokaryotic adaptive immune system. Nature *532*, 385–
462 388.

463 Waldor, M.K., and Mekalanos, J.J. (1996). Lysogenic conversion by a filamentous phage
464 encoding cholera toxin. Science *272*, 1910–1914.

465 Wang, X., Yao, D., Xu, J.-G., Li, A.-R., Xu, J., Fu, P., Zhou, Y., and Zhu, Y. (2016).
466 Structural basis of Cas3 inhibition by the bacteriophage protein AcrF3. Nat. Struct. Mol.
467 Biol. *23*, 868–870.

468 Weigle, J.J., and Delbruck, M. (1951). Mutual exclusion between an infecting phage and
469 a carried phage. J. Bacteriol. *62*, 301–318.

470 Westra, E.R., van Houte, S., Oyesiku-Blakemore, S., Makin, B., Broniewski, J.M., Best,
471 A., Bondy-Denomy, J., Davidson, A., Boots, M., and Buckling, A. (2015). Parasite
472 Exposure Drives Selective Evolution of Constitutive versus Inducible Defense. Curr. Biol.
473 *25*, 1043–1049.

474 Wiedenheft, B., van Duijn, E., Bultema, J.B., Bultema, J., Waghmare, S.P., Waghmare,
475 S., Zhou, K., Barendregt, A., Westphal, W., Heck, A.J.R., et al. (2011). RNA-guided
476 complex from a bacterial immune system enhances target recognition through seed
477 sequence interactions. Proceedings of the National Academy of Sciences *108*, 10092–
478 10097.

479

480 **FIGURE LEGENDS**

481 **Figure 1. Anti-CRISPRs are imperfect CRISPR-Cas inhibitors**

482 **(A)** Efficiency of plaquing (EOP) of 5 related phages bearing distinct *acrIF* genes
483 (JBD30$_{acrIF1}$, MP29$_{acrIF2}$, JBD88a$_{acrIF3}$, JBD24$_{acrIF4}$, LPB1$_{acrIF7}$) on *Pseudomonas*
484 *aeruginosa* strain PA14. Plaque forming units (PFUs) were quantified on wild-type PA14
485 with 1-2 natural targeting spacers (WT + pEmpty) or on PA14 overexpressing 1 targeting
486 spacer (WT + pSp1), then normalized to the number of PFUs measured on a non-
487 targeting PA14 derivative (0sp). Data are represented as the mean of 3 biological
488 replicates +/- SD.

489 **(B)** EOP of isogenic DMS3m phages with *acrIF1-7* or *acrIE3* in the DMS3m *acr* locus.
490 EOP was calculated as PFU counts measured on WT PA14 with 1 targeting spacer
491 (1sp) or a laboratory evolved PA14 derivative with 5 targeting spacers (5sp) normalized
492 to PFU counts measured on non-targeting PA14 (0sp). Data are represented as the
493 mean of 3 biological replicates +/- SD. ND, not detectable.
494 **(C)** Plot of association (Ka) and dissociation (Kd) rates for AcrIF1 (data adapted from
495 Chowdhury et al. 2017) and AcrIF4 binding the PA14 Csy complex. See Figure S2 for
496 SPR AcrIF4 sensogram.
497
498 **Figure 2. Anti-CRISPR success requires cooperative infections during lytic growth**
499 **(A-F)** 12 h growth curves of *P. aeruginosa* strain PA14 with 5 targeting spacers
500 (+CRISPR, panels **A-C**) or no CRISPR-Cas function (ΔCRISPR, **D-F**) infected with
501 virulent variants of DMS3m$_{acrIF1}$, DMS3m$_{acrIF4}$, or DMS3m$_{acrIE3}$ at multiplicity of infection
502 (MOI) increasing in 10-fold steps from $2x10^{-5}$ to $2x10^{1}$ (rainbow colors) or uninfected
503 (black). Phage were harvested after 24 hours and quantified as PFUs on PA14 0sp
504 (horizontal bars). Colors correspond to the MOI legend and growth curves. OD600 and
505 phage output are represented as the mean of 3 biological replicates +/- SD. ND, not
506 detectable.
507 **(G-I)** Replication of virulent DMS3m$_{acr}$ phages (target phage) in the presence of 10^6 PFU
508 (MOI 0.2) hybrid phage (donor) in PA14 with 5 targeting spacers expressing the JBD30
509 C-repressor. Phages were harvested after 24 hours of co-culture and DMS3m$_{acr}$ phage
510 PFUs were quantified on PA14 0sp expressing the JBD30 C repressor. Phage output is
511 represented as the mean of 3 biological replicates +/- SD. ND, not detectable.
512
513 **Figure 3. Immunosuppression facilitates acquisition of a marked prophage**
514 (**A,B**) Acquisition of marked DMS3m$_{acrIF4}$ or DMS3m$_{acrIE3}$ prophage by PA14 with 0
515 spacers (0 sp, circles) or 5 targeting spacers (5 sp, triangles). This experiment was
516 performed in biological triplicate, and individual replicate values are displayed. LoD, limit
517 of detection.
518 (**C,D**) Efficiency of lysogeny (EOL) of DMS3m$_{acrIF4\ gp52::gentR}$ and
519 DMS3m$_{acrIE3\ gp52::gentR}$ in the presence of CRISPR targeting. EOL was calculated by
520 dividing the output lysogens forming units (LFUs) from the strain with 5 targeting spacers
521 (5sp) to the number of LFUs in PA14 with 0 targeting spacers (0sp). Data are
522 represented as the mean of 3 biological replicates +/- SD. ND, not detectable.

523 (**E,F**) EOL of 10^3 LFUs of DMS3m$_{acrIF4\ gp52::gentR}$ and DMS3m$_{acrIE3\ gp52::gentR}$ in the presence
524 of 10^7 PFU of the indicated DMS3m$_{acr}$ phage. Data are represented as the mean of 3
525 biological replicates +/- SD. ND, not detectable. See Figure S6 for lysogen genetic
526 analysis.
527
528 **Figure 4. Cas9 anti-CRISPR AcrIIA4 requires cooperative infection to neutralize**
529 **Type II-A CRISPR immunity**
530 **(A)** 10-fold serial dilutions of DMS3m$_{acrIE3}$ or DMS3m$_{acrIIA4}$ plated on a lawn of
531 *Pseudomonas aeruginosa* strain PAO1 expressing *Streptococcus pyogenes* Type II-A
532 Cas9 (PAO1::SpyCas9) and single guide RNA (+ sgRNA) or non-targeting control (+
533 vector).
534 **(B)** Efficiency of plaquing of DMS3m$_{acrIIA4}$ and DMS3m$_{acrIE3}$ was calculated by normalizing
535 PFU counts on a targeting strain of PAO1::SpyCas9 (+sgRNA) to PFU counts on a non-
536 targeting strain of PAO1::SpyCas9 (+vector). Data are represented as the mean of 3
537 biological replicates +/- SD. ND, not detectable.
538 **(C-F)** 12 hour growth curves of PAO1::spyCas9 expressing a targeting sgRNA (+
539 sgRNA, panels **C-D**) or a non-targeting vector control (+vector, E-F) that were infected
540 with virulent DMS3m$_{acrIIA4}$ or DMS3m$_{acrIE3}$ at multiplicities of infection (MOI, rainbow
541 colors) from $2x10^{-5}$ to $2x10^{-2}$. Growth curves of uninfected cells are shown in black.
542 Phage were harvested after 24 hours and PFUs quantified on PAO1::SpyCas9 + vector
543 (horizontal bars). OD600 and phage output are represented as the mean of 3 biological
544 replicates +/- SD.
545 **(G-H)** Replication of virulent DMS3m$_{acr}$ phages (target phage) in the presence of 10^7
546 PFU (MOI 2) hybrid phage (donor) in PAO1::SpyCas9 + sgRNA expressing the JBD30
547 C-repressor. Phages were harvested after 24 hours and DMS3m$_{acr}$ phage PFUs
548 quantified on PAO1::SpyCas9 + vector expressing the JBD30 C repressor. Phage output
549 is represented as the mean of 3 biological replicates +/- SD. ND, not detectable.
550
551 **Figure 5. Phage cooperation to suppress CRISPR-Cas immunity**
552 *Left*: Failed infections generate an immunosuppressed cell. While the phage genome
553 may be cleaved (dashed red line), Acr protein (small cyan circles) will be produced,
554 binding to some CRISPR-Cas complexes (larger purple structures, with crRNA). *Right:*
555 At low parasite density, it is unlikely the cell will be re-infected and the host will survive.
556 As high parasite density, the likelihood that the immunosuppressed cell with be re-

557 infected is higher. Co- or re-infection will lead to successful parasite replication and
558 amplification of the infectious population.
559
560 **SUPPLEMENTAL FIGURE LEGENDS**
561 **Figure S1. Engineering DMS3m$_{acr}$ phages**
562 **(A)** Schematic of two *acr* locus architectures used to generate an isogenic family of
563 DMS3m$_{acr}$ phages.
564 **(B)** Efficiency of plaquing (EOP) of DMS3m$_{acrIF1}$ with natural or synthetic locus
565 architecture on PA14 with 1 or 5 targeting spacers (1sp and 5 sp). Data are represented
566 as the mean of 3 biological replicates +/- SD.
567 **(C)** Table of DMS3m$_{acr}$ phage genotype and locus architecture, as well as the original
568 source of the *acr* gene and the corresponding accession number of the Acr protein.
569
570 **Figure S2. Sensograms of AcrIF4 and AcrIF1 binding the Csy complex**
571 **(A)** Sensogram showing real-time binding of increasing concentrations of free AcrIF4
572 (1.85 nM, 55.6 nM, 167 nM, 500 nM, 1.5 μM) to immobilized Csy complex. A model
573 describing Langmuir binding (black line) was fit to the data to calculate binding constants
574 (Ka, Kd, and KD; boxed inset).
575 **(B)** Sensogram showing real-time binding of increasing concentrations of free AcrIF1
576 (1.85 nM, 55.6nM, 167 nM, 500 nM, 1.5 μM) to immobilized Csy complex. A model
577 describing binding at a 2:1 stoichiometry of free analyte:immobilized ligand (black line)
578 was fit to the data to calculate binding constants (Ka1, Ka2,
579 Kd1, Kd2, and KD1, KD2; boxed inset) (Chowdhury and et al. 2017).
580
581 **Figure S3. Output phages from Figure 1B are CRISPR sensitive**
582 Efficiency of plaquing (EOP) of the original stock of virulent DMS3macr$_{IF4}$ (input) on
583 PA14 5 sp compared to EOP of DMS3m$_{acrIF4}$ harvested from high MOI infections (MOI 2,
584 MOI 20 output) from figure 2B. Data are represented as the mean of 3 biological
585 replicates +/- SD.
586
587 **Figure S4. Generating and validating Hybrid$_{acr}$ phages**
588 **(A)** 10-fold serial dilutions of DMS3m$_{acrIE3}$ and JBD30$_{acrIF1}$ spotted on lawns of non-
589 targeting (0sp) *Pseudomonas aeruginosa* PA14 expressing the DMS3m C repressor
590 (*gp1-DMS3m*), the JBD30 C repressor (*gp1-JBD30*) or a vector control.

591 **(B)** 10-fold serial dilutions of hybrid DMS3m$_{acrIE3\ gp1\text{-}JBD30}$ plated on lawns of non-targeting
592 (0sp) *Pseudomonas aeruginosa* PA14 expressing the DMS3m C repressor (*gp1-*
593 *DMS3m*), the JBD30 C repressor (*gp1-JBD30*), or a spacer which uniquely targets
594 JBD30 (2sp17).
595 **(C)** Hybrid phage (Hybrid$_{acrIF1}$ or Hybrid$_{acrIE3}$) harvested from infections of PA14 5sp
596 expressing the JBD30 C repressor from experiments shown in Figure 2G-I. Hybrid PFUs
597 were quantified on the 0sp PA14 strain. Data are represented as the mean of 3
598 biological replicates +/- SD.
599 **(D)** 10-fold serial dilutions of JBD30$_{acrIF1}$ or virulent DMS3m$_{acrIE3}$ spotted on lawns of
600 PA14 Δ*csy3* or PA14 Δ*csy3* lysogenized with Hybrid$_{acrIE3}$ or Hybrid$_{acrIF1}$. Despite being
601 heteroimmune with respect to DMS3, the DMS3 phage is unable to replicate well on this
602 lysogens due to other superinfection exclusion properties of DMS3.
603
604 **Figure S5. Timecourse of lysogen formation**
605 Time course of acquisition of gentamicin-resistance marked DMS3m$_{acrIFI\ gp52::gentR}$
606 prophage by a non-targeting (0 sp) strain of PA14, labeled with estimates of each
607 infectious cycle (Rounds 1-3). Data are represented as the mean of 3 biological
608 replicates +/- SD.
609
610 **Figure S6. Prophage content of lysogens from Figure 3E-F**
611 **(A)** 10-fold serial dilutions of supernatant harvested from overnight cultures of lysogens
612 from Figure 3E (1-48) and 3F (49-51), spotted on a non-targeting (0 sp) strain of PA14. A
613 faint clearing corresponds to induction of the gentamicin marked phage, while strong
614 plaquing (i.e. 50, 51) reflects the presence of the gentamicin marked phage and the
615 helper phage.
616 (**B**) PCR of genomic DNA harvested from harvested from overnight cultures of lysogens
617 from Figure 3E (1-48) and 3F (49-51) amplified with primers targeting *gp52-DMS3m* (top) or
618 the gentamicin resistance cassette used to replace *gp52* in *DMS3m*$_{acr\ gp52::gentR}$ derivatives
619 (bottom).
620
621 **METHODS**
622 **Strains and growth conditions**
623 *Pseudomonas aeruginosa* strains (UCBPP-PA14, PAO1) and *Escherichia coli* strains
624 were cultured on lysogeny broth (LB) agar or liquid media at 37C. LB was supplemented
625 with gentamicin (50 µg/mL for *P. aeruginos*a, 30 µg/mL for *E. coli*) to maintain the

626 pHERD30T plasmid or carbenicillin (250 µg/mL for *P. aeruginosa*, 100 µg/mL for *E. coli*)
627 to maintain pHERD20T or pMMBHE. To maintain pHERD30T and pMMBHE in the same
628 strain of *P. aeruginosa*, double selection of 30 µg/mL gentamicin and 100 µg/mL
629 carbenicillin was employed. In all *P. aeruginosa* experiments, expression from
630 pHERD20/30T was induced with 0.1%
631
632 **PAO1 SpyCas9 expression strain**
633 SpyCas9 expressed from the P_{LAC} promoter of pUC18T-mini-Tn7T-Gm was integrated
634 into the *P. aeruginosa* strain PAO1 chromosome by electroporation and Flp-mediated
635 marker excision as previously described (Choi and Schweizer, 2006). To generate the
636 heterologous Type II-A PAO1 strain the PAO1-attTn7::pUC18T-miniTn7T-P_{LAC}-SpyCas9
637 strain was transformed with pBAO72 (pMMB67HE-P_{LAC}-sgRNA) by electroporation. In all
638 experiments with this strain, SpyCas9 and the sgRNA were induced with 1mM IPTG.
639
640 **Construction of recombinant DMS3m$_{acr}$ phages**
641 DMS3m$_{acrIF1}$ was generated as in (Bondy-Denomy et al., 2013) by infecting cells
642 containing a recombination plasmid bearing JBD30 genes 34-38 (the anti-CRISPR locus
643 with large flanking regions). JBD30 naturally carries *acrIF1* and has high genetic
644 similarity to DMS3m$_{acrIE3}$, permitting for the selection of recombinant DMS3m phage
645 which had acquired *acrIF1*. To generate the extended panel of DMS3m$_{acr}$ phages in this
646 work, recombination cassettes were generated with regions from up and downstream the
647 anti-CRISPR genes from JBD30 Gibson assembled to flank the *acr* gene of interest on
648 pHERD20T or pHERD30T (see S1 for *acr* gene sources and exact details of *acr* locus
649 architecture). Recombinant phages were generated by infecting cells bearing these
650 recombination substrates. DMS3m$_{acr}$ phages were screened for their ability to resist
651 CRISPR targeting, and the insertion of the anti-CRISPR gene was confirmed by PCR.
652 Virulent derivatives of DMS3m$_{acr}$ phages were constructed by deleting gp1 (C repressor)
653 using materials and methods from Cady et al., 2012.
654
655 **Construction of DMS3m$_{acr\ gp52::GentR}$ phages**
656 A recombination substrate with a gentamicin resistance cassette flanked by homology
657 arms matching the DMS3m genome up and downstream of gp52 (450 bp and 260 bp,
658 respectively) was assembled into pHERD20T using Gibson assembly. This
659 recombination cassette was transformed into PA14 ΔCRISPR lysogenized with either
660 DMS3m$_{acrIE3}$ or DMS3m$_{acrIF1}$.These transformed lysogens were grown under gentamicin
661 selection for 16 h, then sub-cultured 1:100 into LB with gentamicin and 0.2 µg/mL
662 mitomycin C to induce the DMS3m$_{acr}$ prophage. Supernatants were harvested after 24
663 hours of induction, and used to infect PA14 ΔCRISPR for 24 h. These cells were then
664 plated on gentamicin plates to select for cells that had acquired a prophage bearing the
665 gentamicin resistance cassette, and gentamicin resistant lysogens were then re-induced
666 with 0.2 µg/mL mitomycin C to recover the recombinant phage.
667
668 **Construction of DMS3m$_{acr\ gp1\text{-}JBD30}$ (Hybrid$_{acr}$) phages**
669 DMS3m$_{acrIE3}$ and JBD30$_{acrIE3}$ were used to co-infect PA14 ΔCRISPR and the infected
670 cells were mixed with molten top agar and poured onto solid plates. After 24 hours of
671 growth at 30C, the phages were harvested by flooding the plate with SM buffer and
672 collecting and clarifying the supernatant. Phages were then used to infect PA14
673 ΔCRISPR expressing the DMS3 C repressor from pHERD30T, and the infections were
674 mixed with molten top agar and poured onto solid plates. After 24 hours of growth at 30
675 ºC, individual plaques with DMS3 morphology were picked, purified 3x by passage in
676 PA14 ΔCRISPR and screened as shown in Figure S4B.

677
678 **Phage (PFU) quantification**
679 Phage plaque forming units (PFU) were quantified by mixed 10µl of phage at a with 150
680 µl of an overnight culture of host bacteria. The infection mixture was incubate at 37 ºC
681 for 10 minutes to promote phage adsorption, then mixed with 3 mLs molten top agar and
682 spread on an LB agar plate supplemented with 10 mM $MgSO_4$. After 16 hours of growth
683 30 ºC, PFUs were quantified.
684
685 **Phage titering**
686 A bacterial lawn was generated by spreading 3 mLs of top agar seeded with 150 µl of
687 host bacteria on a LB agar plate supplemented with 10 mM $MgSO_4$. 3 µl of phage
688 serially diluted in SM buffer was then spotted onto the lawn, and incubated at 30 ºC for
689 16 hours.
690
691 **Measurement of anti-CRISPR binding kinetics by surface plasmon resonance**
692 Purified Csy complex was covalently immobilized by amine coupling to the surface of a
693 carboxymethyldextran-modified (CM5) sensor chip. Purified 6his-tagged AcrIF4 was
694 injected into the buffer flow in increasing concentrations (1.85 nM, 55.6 nM, 167 nM, 500
695 nM, 1.5 uM), and Csy complex-AcrIF4 binding events were recorded in real time.
696 Experiments were conducted at 37°C, in 20 mM HEPES pH 7.5, 100 mM KCl, 1mM
697 TCEP, 0.005% Tween. Data were fit with a model describing Langmuir binding (i.e. 1:1
698 binding between free analyte and immobilized ligand). Kinetic rate constants were
699 calculated using Biacore evaluation software (GE).
700
701 **Liquid culture phage infections**
702 Liquid culture phage infections and growth curves were performed by infecting 140 µl of
703 *P. aeruginosa* 1:100 diluted overnights cultured in LB supplemented with 10 mM MgSO4
704 and antibiotics and inducer in a 96 well costar plate with 10 µl of phage diluted in SM
705 buffer. These infections proceeded for 24 hours in a BioTek Synergy microplate reader
706 at 37 ºC with continuous shaking. After 24 hours, phage was extracted treating each
707 sample with chloroform followed by centrifugation at 21,000 x g for 2 minutes.
708
709 **Lysogen acquisition and induction**
710 Overnight cultures of PA14 were subcultured at 1:100 for ~3 hours (OD_{600nm} = 0.3) in LB
711 supplemented with 10 mM MgSO4. 1 mL of cells were then infected with 10 µl DMS3m$_{acr}$
712 $_{gp52::GentR}$ and incubated for 50 minutes at 37 ºC, shaking at 100 rpm. The sample was
713 then treated with a 10% volume of 10X gentamicin, spun down at 8,000xg, and
714 resuspended in 200 ul of LB with 50 µg/mL gentamicin. 100 ul of sample was then plated
715 (after further dilution, if required) on gentamicin selection plates and incubated at 37 ºC.
716 To analyze the lysogens, the resulting colonies were grown for 16 hours in LB + 10 mM
717 MgSO4 (no selection), the supernatants harvested, and serial dilutions spotted onto a
718 lawn of PA14 ΔCRISPR. Crude genomic DNA for PCR analysis was harvested from the
719 lysogens by boiling 10 µl of culture in 0.02% SDS for 10 minutes.
720
721 **Lysogen PCR**
722 PCR amplification of 2 µl of crude genomic DNA harvested from lysogens was used to
723 screen for the presence of *DMS3m-gp52* and *gentR* using MyTaq (Bioline) polymerase
724 with MyTaq GC buffer under standard conditions.
725

Figure 1

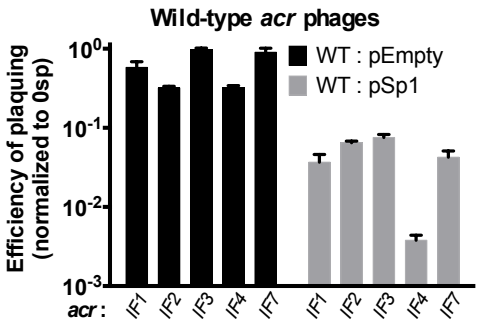
A
Wild-type acr phages
Efficiency of plaquing (normalized to 0sp)
WT : pEmpty
WT : pSp1
acr :
IF1
IF2
IF3
IF4
IF7

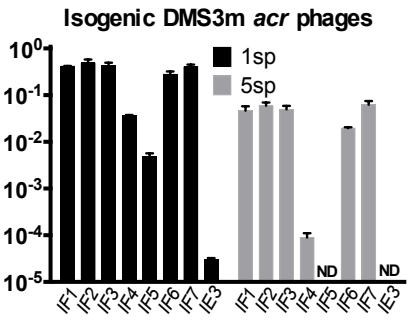
B
Isogenic DMS3m acr phages
1sp
5sp
ND
IF1
IF2
IF3
IF4
IF5
IF6
IF7
IE3

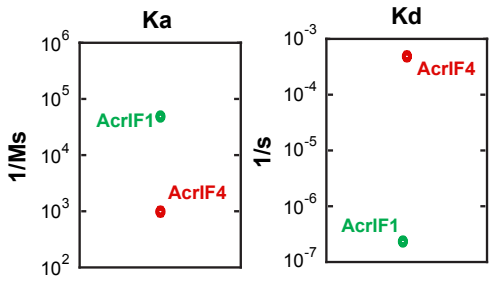
C
Ka
Kd
1/Ms
1/s
AcrIF1
AcrIF4

Figure 2

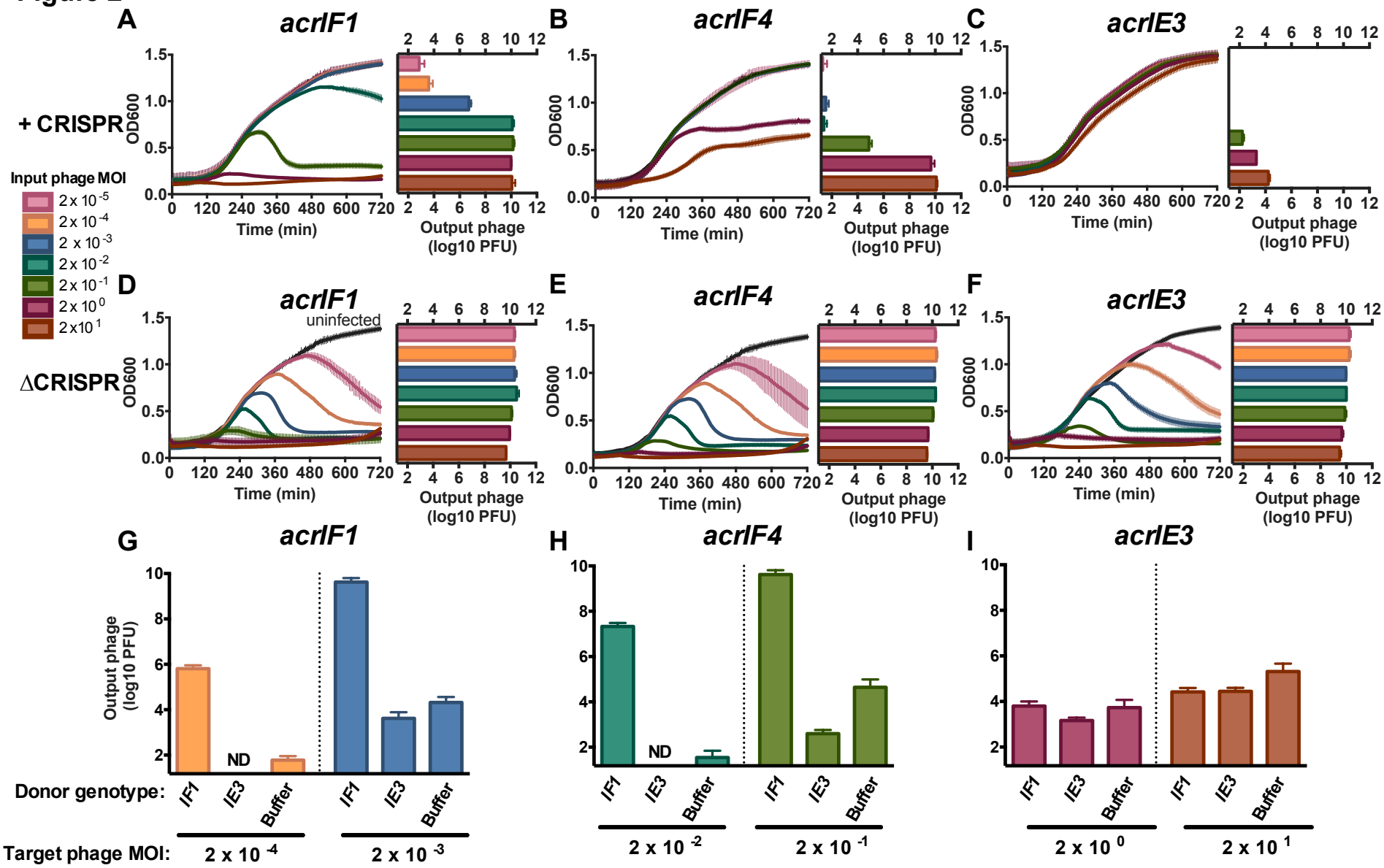
A
acrIF1
B
acrIF4
C
acrIE3
+ CRISPR
Input phage MOI
2 x 10 -5
2 x 10 -4
2 x 10 -3
2 x 10 -2
2 x 10 -1
2 x 10 0
2 x 10 1
D
E
F
ΔCRISPR
uninfected
OD600
Time (min)
Output phage (log10 PFU)
G
H
I
Output phage (log10 PFU)
ND
Donor genotype:
IF1
IE3
Buffer
Target phage MOI:
2 x 10 -4
2 x 10 -3
2 x 10 -2
2 x 10 -1
2 x 10 0
2 x 10 1

Figure 3

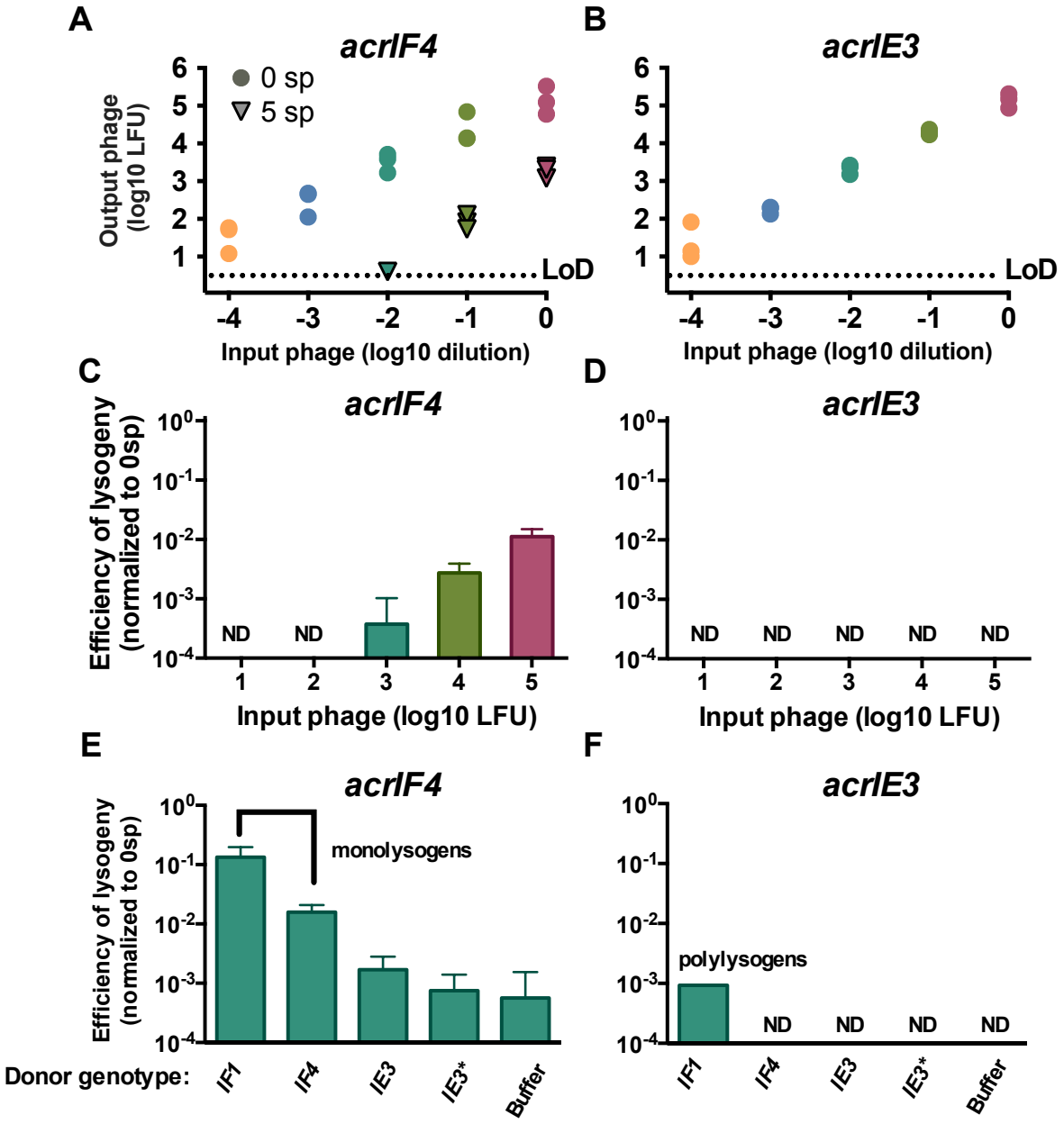
A
acrIF4
0 sp
5 sp
Output phage (log10 LFU)
LoD
Input phage (log10 dilution)
B
acrIE3
LoD
Input phage (log10 dilution)
C
acrIF4
Efficiency of lysogeny (normalized to 0sp)
ND
ND
Input phage (log10 LFU)
D
acrIE3
ND
ND
ND
ND
ND
Input phage (log10 LFU)
E
acrIF4
monolysogens
Efficiency of lysogeny (normalized to 0sp)
Donor genotype:
IF1
IF4
IE3
IE3*
Buffer
F
acrIE3
polylysogens
ND
ND
ND
ND
IF1
IF4
IE3
IE3*
Buffer

Figure 4

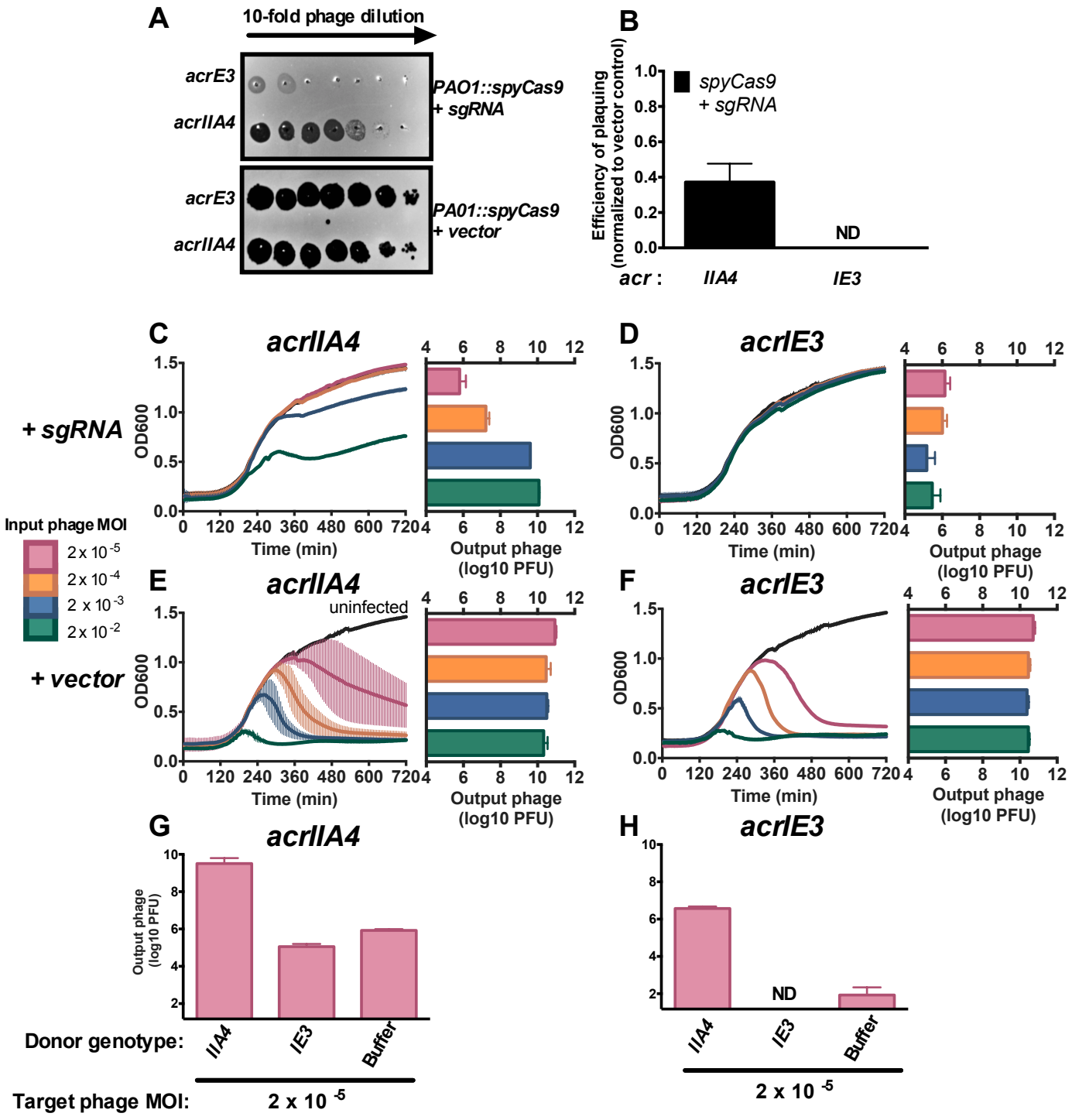
A
10-fold phage dilution
acrE3
acrIIA4
PAO1::spyCas9
+ sgRNA
acrE3
acrIIA4
PA01::spyCas9
+ vector
B
Efficiency of plaquing
(normalized to vector control)
spyCas9
+ sgRNA
ND
acr :
IIA4
IE3
C
acrIIA4
+ sgRNA
OD600
Time (min)
Output phage
(log10 PFU)
D
acrIE3
Input phage MOI
2 x 10 -5
2 x 10 -4
2 x 10 -3
2 x 10 -2
E
acrIIA4
uninfected
+ vector
F
acrIE3
G
acrIIA4
Output phage
(log10 PFU)
Donor genotype:
IIA4
IE3
Buffer
Target phage MOI:
2 x 10 -5
H
acrIE3
ND
IIA4
IE3
Buffer
2 x 10 -5

Figure 5

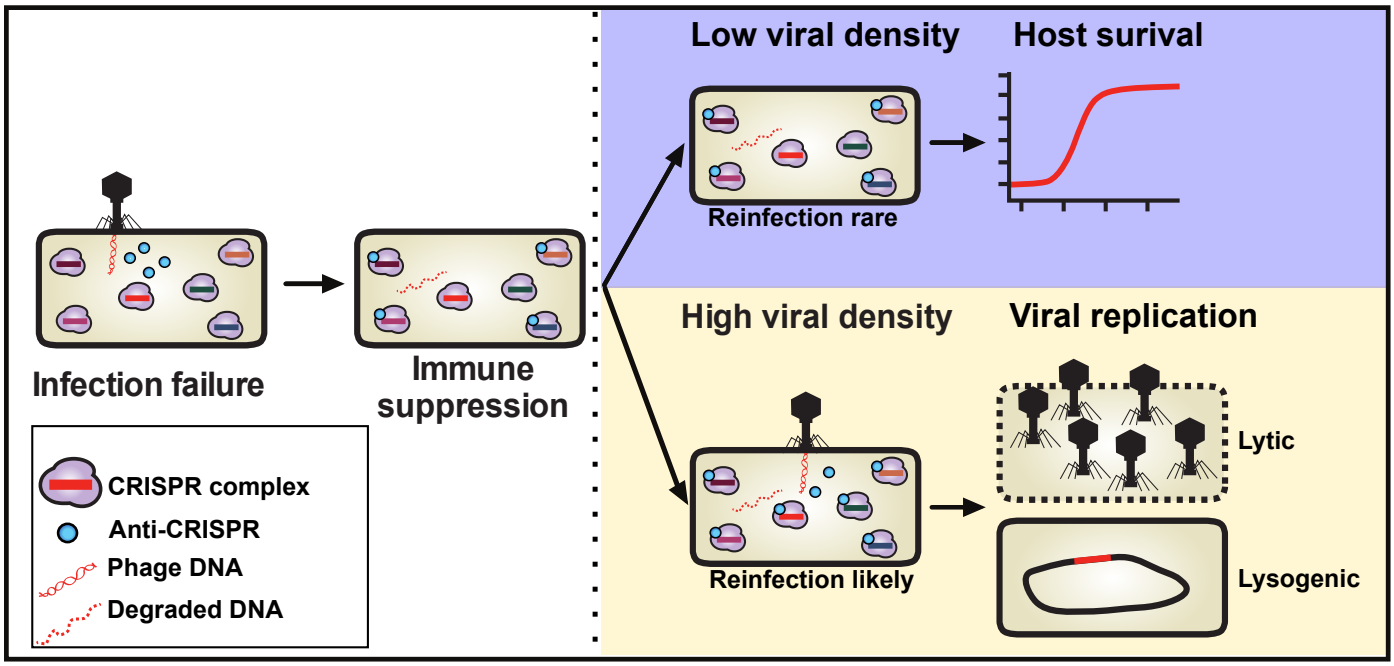
Low viral density
Host surival
Reinfection rare
Infection failure
Immune suppression
High viral density
Viral replication
Lytic
Reinfection likely
Lysogenic
CRISPR complex
Anti-CRISPR
Phage DNA
Degraded DNA

Supplementary Figure 1

A

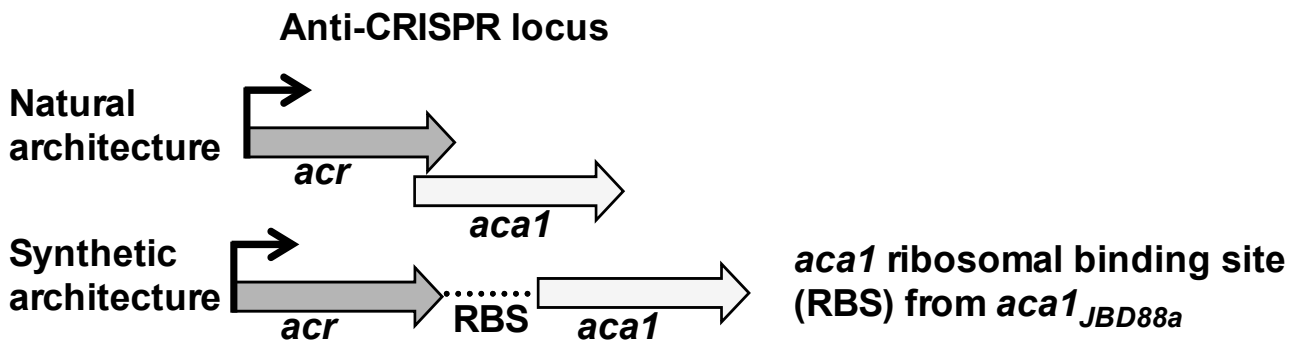

B

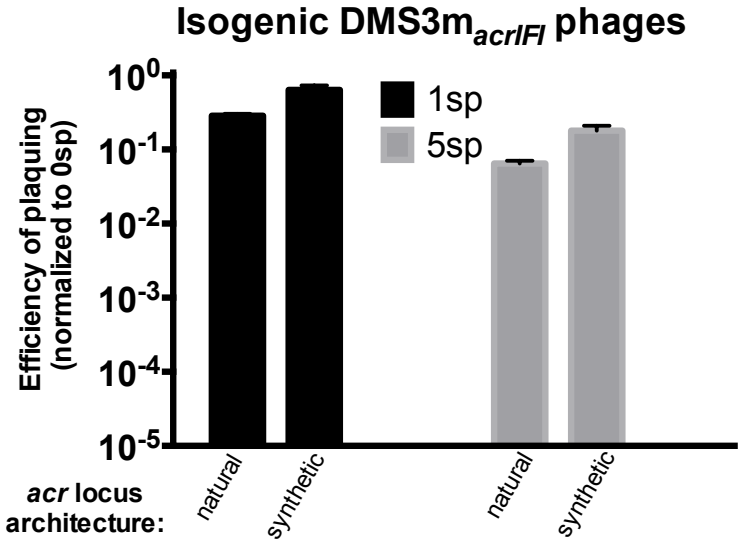

C **DMS3m$_{acr}$ phages**

Phage	DMS3m$_{acr}$ architecture	*acr* gene source	Acr Accession
DMS3m$_{acrIE3}$ (parent phage, no manipulation)	natural	DMS3m (gp30)	WP_003723290.1
DMS3m$_{acrIF1}$	natural	JBD30 (gp35)	YP_007392342.1
DMS3m$_{acrIF2}$	natural	MP29 (gp29)	YP_002332454.1
DMS3m$_{acrIF3}$	natural	JBD88a (gp33)	YP_007392440.1
DMS3m$_{acrIF4}$	natural	JBD26 (gp37)	WP_016068584.1
DMS3m$_{acrIF5}$	synthetic	JBD5 (gp36)	YP_007392740.1
DMS3m$_{acrIF6}$	synthetic	*Pseudomonas aeruginosa* strain PSE05 (prophage)	WP_043884810.1
DMS3m$_{acrIF7}$	natural	LPB1 (gp29)	YP_009146150.1
DMS3m$_{acrIIA4}$	synthetic	*Listeria monocytogenes* J0161 (prophage)	WP_003723290.1

Supplementary Figure 2

A

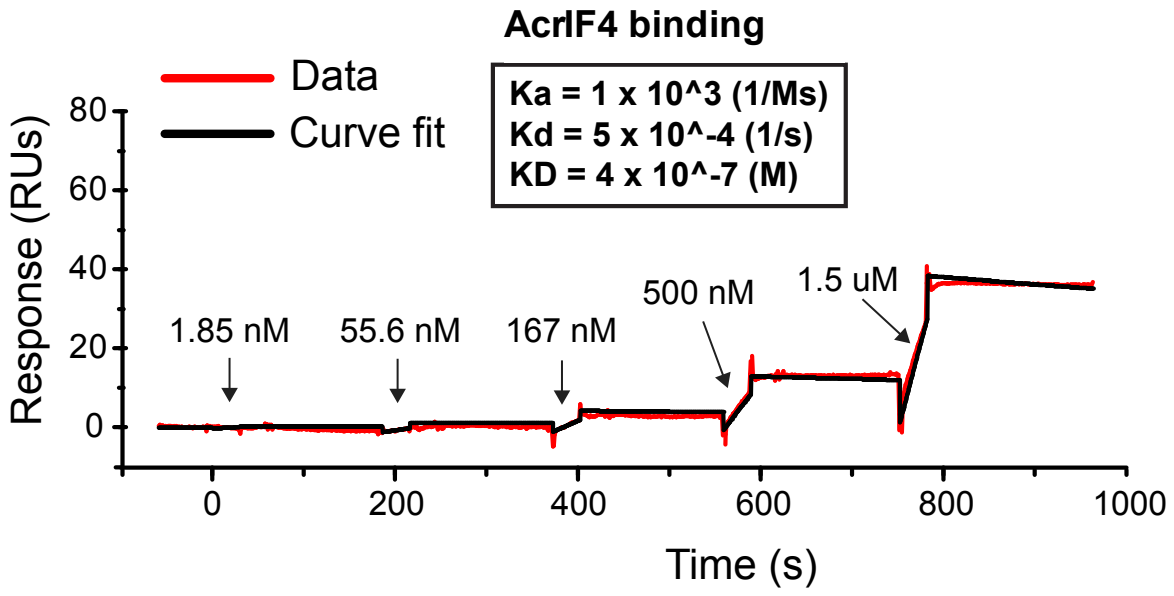

Supplementary Figure 3

A

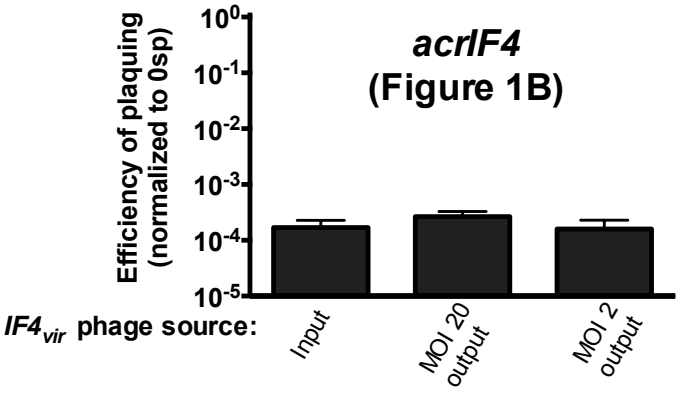

Supplementary Figure 4

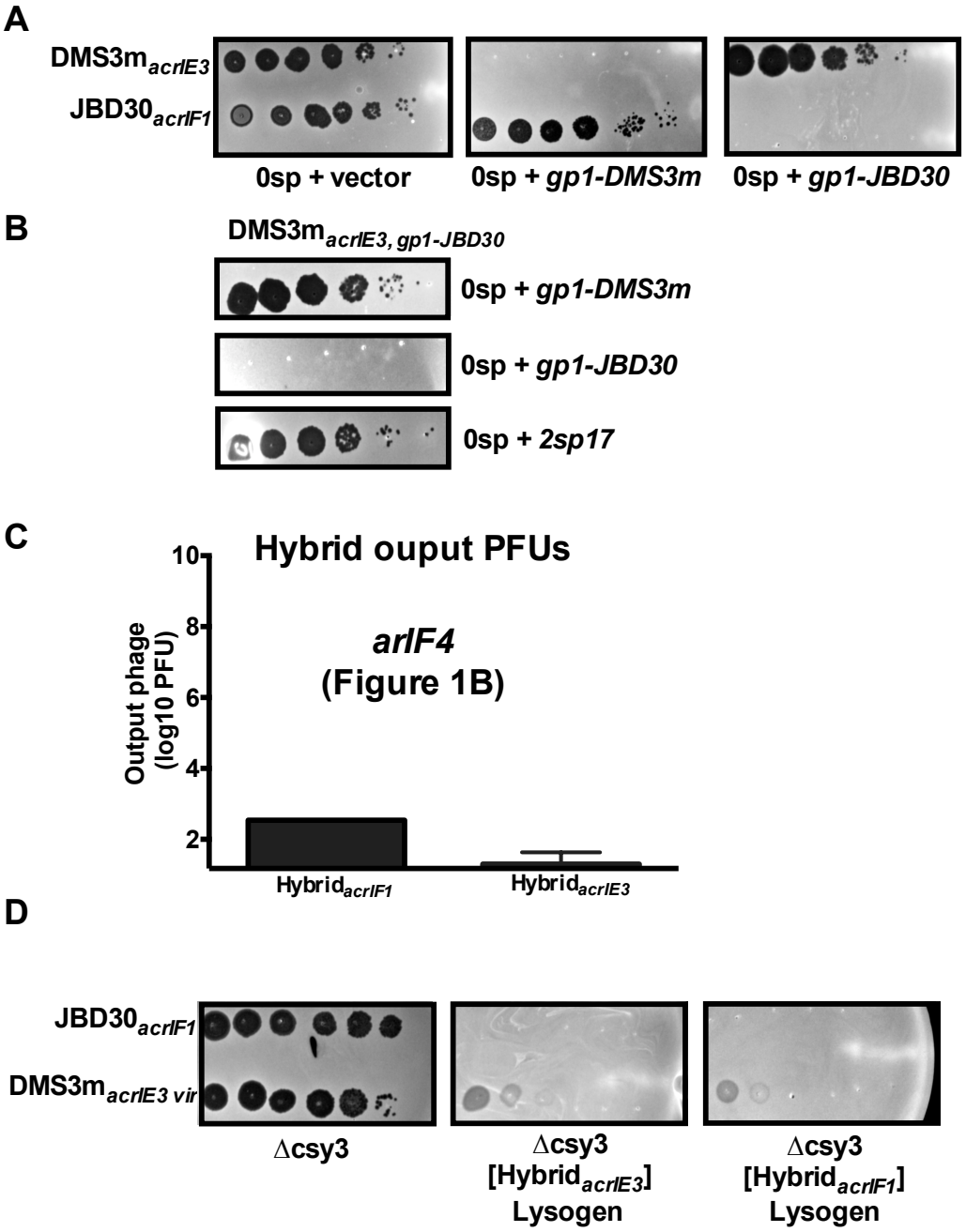

Supplementary Figure 5

A

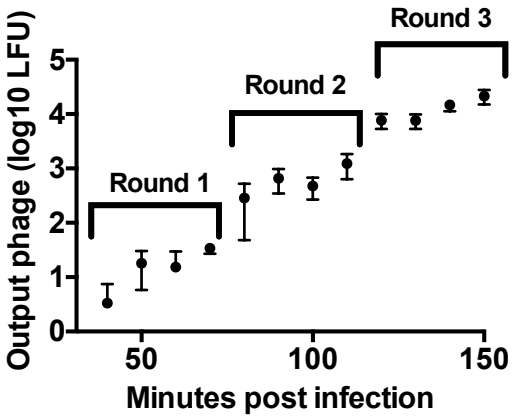
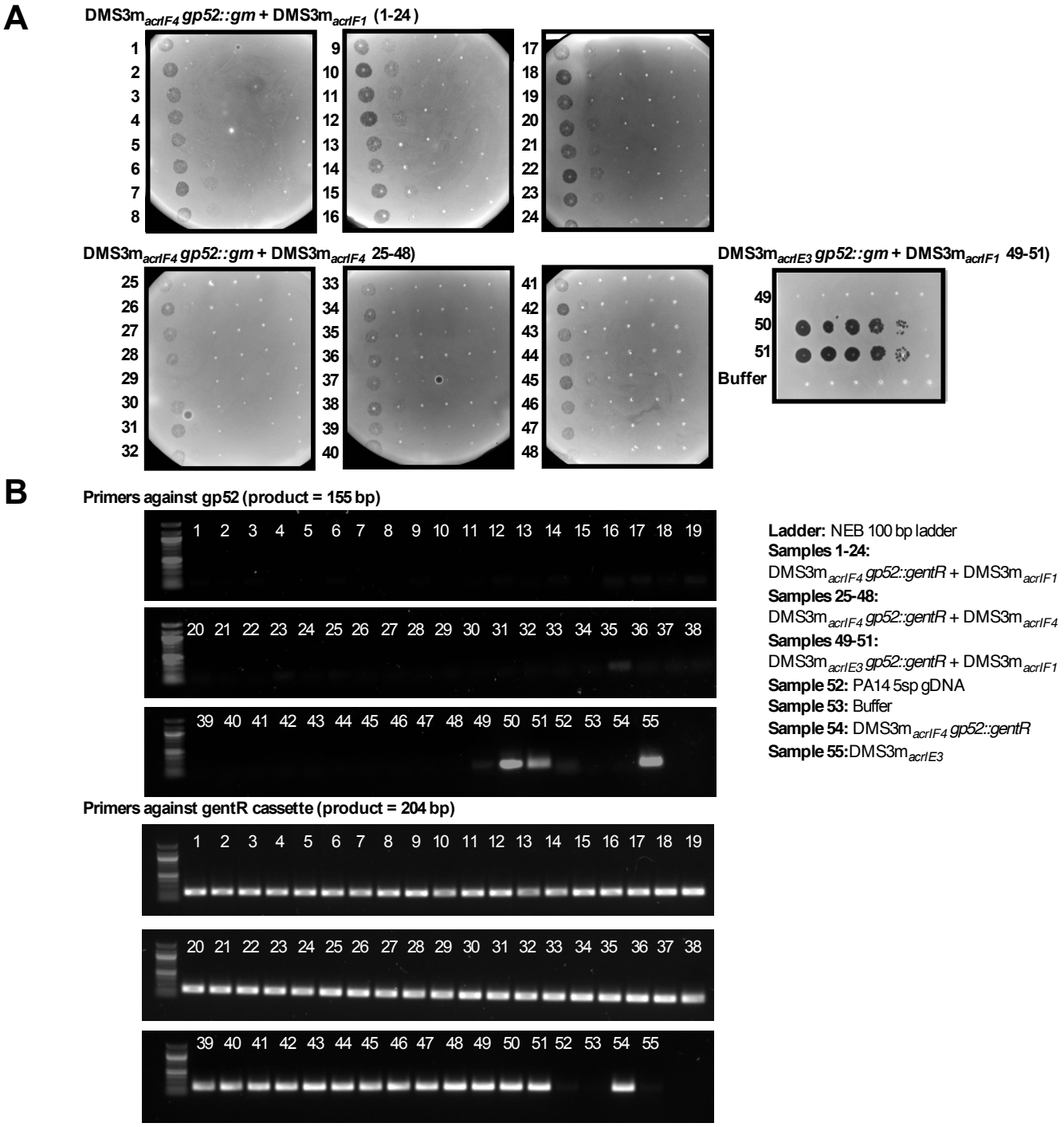
Supplementary Figure 6